

Colloidal atomic layer deposition on nanocrystals using ligand-modified precursors

Philippe Green

École polytechnique fédérale de Lausanne

Ona Segura Lecina

École polytechnique fédérale de Lausanne

Petru Albertini

École polytechnique fédérale de Lausanne

Mark Newton

ETH <https://orcid.org/0000-0002-6389-2144>

Krishna Kumar

École polytechnique fédérale de Lausanne

Coline Boulanger

École polytechnique fédérale de Lausanne

Jari Leemans

EPFL

Paul Thompson

University of Liverpool

Anna Loiudice

École Polytechnique Fédérale de Lausanne

Raffaella Buonsanti

`raffaella.buonsanti@epfl.ch`

École Polytechnique Fédérale de Lausanne <https://orcid.org/0000-0002-6592-1869>

Article

Keywords:

Posted Date: January 3rd, 2024

DOI: <https://doi.org/10.21203/rs.3.rs-3792425/v1>

License:   This work is licensed under a Creative Commons Attribution 4.0 International License.

[Read Full License](#)

Additional Declarations: There is **NO** Competing Interest.

Version of Record: A version of this preprint was published at Journal of the American Chemical Society on April 5th, 2024. See the published version at <https://doi.org/10.1021/jacs.4c00538>.

Abstract

Atomic layer deposition (ALD) is a method to grow thin metal oxide layers on a variety of materials for applications spanning from electronics to catalysis. Extending ALD to colloiddally stable nanocrystals promises to combine the benefits of thin metal oxide coatings with the solution processability of nanocrystals. However, challenges persist in applying this method, which relate to finding precursors that promote growth of the metal oxide while preserving colloidal stability throughout the process. Herein, we introduce a colloidal ALD method to coat nanocrystals with amorphous metal oxide shells using metal and oxygen precursors that act as colloiddally stabilizing ligands. Our scheme, involves metal-amide precursors modified with solubilizing groups and oleic acid as the oxygen source. The growth of the oxide is self-limiting and proceeds in a layer-by-layer fashion. Our protocol is generalizable and intrinsically scalable. Potential applications in display, light detection and catalysis are envisioned.

Introduction

Gas phase atomic layer deposition (ALD) relies on two self-limiting half reactions to grow atomically precise thicknesses of a variety of materials on solid substrates.¹⁻³ Such an atomic level of control has spurred extensive industrial and fundamental efforts for the assembly of optoelectronic and catalytic devices.² The translation of this approach to colloiddally stable substrates, such as nanocrystals (NCs), would combine the advantages derived from such coatings with the solution processability of NCs, which is sought after in advanced manufacturing.

A colloidal derivative of ALD (c-ALD) was introduced by Ithurria et al. through the development of a self-limited growth of CdS layers on CdSe NCs.⁴ This approach relies on the sequential transfer of NCs between polar and non-polar solvents, isolating the two half reactions in each solvent to achieve layer-by-layer growth of metal-chalcogenide shells.^{4,5} Extending c-ALD to the growth of amorphous metal oxides is desirable as such coatings would provide photo- and environmental protection while not imposing detrimental geometric strain to the nanocrystalline core, properties that are needed for optoelectronic devices.⁶⁻¹³

Recently, a c-ALD methodology was introduced to grow thin metal oxide coatings through an initial half reaction with a highly reactive alkylmetal precursor followed by the introduction of water, O₂ or isopropanol as the second half reaction.¹⁴⁻¹⁶ This scheme resulted in the formation of hybrid shells, in which the organic ligands become integral components of the grown metal oxide.^{11,17} This structure offers new opportunities in the design of multifunctional materials for applications in photocatalysis, incoherent photon conversion¹⁷ and electrocatalysis¹⁶. However, these hybrid oxide shells are not readily amenable to solid-state optoelectronic devices, where ligands are commonly removed to promote electronic transport in dense NC films.¹⁸ Consequently, a scheme needs to be developed that result in fully inorganic coatings.

Herein, we propose a c-ALD scheme which creates a fully inorganic metal oxide coating on the NCs. Key to this method is the use of precursors that are simultaneously reactive towards the NC surface and provide colloidal stabilization. First, we demonstrate that metal-amides react with bound carboxylates, resulting in the direct anchoring of the precursor to the NC surface. On this basis, we develop a scheme where metal-amides are functionalized with solubilizing groups; then, we use oleic acid as both a ligand and oxygen source to grow metal oxide shells. Through ^1H nuclear magnetic resonance (NMR) and X-ray absorption spectroscopy (XAS) measurements, we probe the nucleation and growth of the shell and show that the developed scheme successfully removes all of the native ligands and results in the formation of an amorphous inorganic shell. We demonstrate our claims by growing gallium oxide and titanium oxide shells on a variety of nanocrystalline compositions. This approach results in the successful growth of thin amorphous oxides, which is envisioned as ideal for NC based solid-state optoelectronic devices.

Results and discussion

We studied the interaction of five typical ALD precursors for the growth of metal oxides by c-ALD on carboxylate passivated NC surfaces.^{2,19} We opted for alkyl-metals and metal-amides as they are soluble in non-polar solvents and their expected byproducts should not interfere with shell formation. We selected trimethylgallium (TM-Ga), dimethyl zinc (DM-Zn), trimethyl aluminium (TM-Al), tris(dimethylamido)gallium (TDMA-Ga) and tetrakis(dimethylamido)titanium (TDMA-Ti), as a representative set to contrast the interaction strength of each precursor (**Supplementary Fig. 1**).^{19,20}

For the purpose of this study, we elected to focus mainly on PbS NCs, as they are valuable for a variety of optoelectronic applications and their surface chemistry is well-established.^{21,22} We also opted to grow metal oxide shells on InP NCs, CdSe nanoplatelets (NPLs) and NaGdF₄ NCs as they are recognized alternatives in display, lasing, and biological imaging but face persistent issues in terms of stability.^{23–26} We synthesized PbS NCs (spheres and cubes), InP NCs, CdSe NPLs and NaGdF₄ NCs all capped by oleate ligands through previously established protocols (**Supplementary Figs. 2–12**).^{26–30}

Figure 1a-e reports ^1H NMR spectra which track changes in the alkene resonance of bound oleates on PbS NCs while titrating the c-ALD precursor.³¹ During each titration, a new resonance upfield to the alkene resonance emerges, which indicates an interaction of the precursors with the oleate ligands. Titrations were arrested when precipitation of the NCs occurred. We compared the amount of displaced/transformed oleates from the surface per equivalents of added precursor (**Supplementary Figs. 13–22**), which we used as a metric to quantify the strength of interaction between the ALD precursors and the oleate ligands. Based on such quantification, we established a reactivity trend among the precursors: TM-Al > DM-Zn \geq TM-Ga < TDMA-Ga < TDMA-Ti (Fig. 1, **Supplementary Note 1**).

Drawing parallels with gas phase ALD on polymers^{32–35}, we consider that an adduct forms between the Lewis acidic metal precursors and the Lewis basic carbonyls of bound oleates. TM-Al is a harder Lewis acid than TM-Ga and DM-Zn.³⁶ Thus, TM-Al is expected to interact more strongly with the bound oleates

compared to the other two methyl-based precursors. Through the same principle, it is anticipated that the harder Lewis acidity of TDMA-Ti compared to TDMA-Ga rationalizes the larger release of oleates for the former. Finally, the larger displacement observed for TDMA-Ga compared to TM-Ga correlates well with the harder character of the amide ligands compared to the methyl groups, effectively hardening the precursor and making it more reactive towards the bound oleates.

We then sought to identify the chemical species generating the new ^1H NMR resonances. Based on a suite of 1D and 2D NMR characterization, alkyl-metals result in the formation of cluster-like species (**Supplementary Figs. 23–31**), which do not interact with the NC surface. These cluster-like species are known to assemble from such precursors and metal-carboxylates.^{37–40} Instead, when using metal amide precursors, we found sharp resonances (Fig. 1f, **Supplementary Figs. 32–40**), that correspond to dimethyl oleamides.^{41,42} The presence of this species is consistent with an amidation reaction between the precursor and the surface oleate, which results in the formation of dimethyl oleamide and of a Pb-O-M (M = Ti or Ga) bond on the surface of the PbS NCs (Fig. 1g).³² Thus, metal-amide precursors react with surface oleate to directly anchor the precursor to the NC surface by transforming the starting ligands into species which do not interact with the NC surface.

Having learned that all the metal precursors do interact with the surface of the oleate-capped PbS NCs, we proceeded in growing the oxide shell according to the previously reported c-ALD method, which yields hybrid oxide shells with embedded oleate ligands.^{14,16} Each precursor lead to the formation of such shells on the NCs, with the exception of TM-Ga (**Supplementary Figs. 41–43**), which is consistent with the reported reactivity scale. This latter issue can be circumvented by having an alumina layer initially present, exploiting the higher reactivity of TM-Al to seed gallium oxide formation (**Supplementary Figs. 44–45**). Further, only dilute and sub-stoichiometric amounts of the precursors can be employed in this method without causing loss of colloidal stability of the NCs. This limitation results in a partial coverage of the NC surface by the oxide layer for each cycle. To expand the scope of this previous methodology and yield a fully inorganic interface between the NC and the oxide shell, we reasoned that both the precursor and oxygen source needed to be colloiddally solubilizing ligands.

To this end, we developed a methodology that relies upon the observation of dimethyl oleamide and Pb-O-M bond formation during the addition of metal-amide precursors. We first sought to endow the metal precursor with colloiddally solubilizing functionalities (*i.e* make it a good ligand). Thus, we performed a transamidation reaction to partially replace the short destabilizing dimethylamide with solubilizing didodecylamides (Fig. 2a, **Supplementary Figs. 46–47, Supplemental Note 2**).⁴⁴ Further, we noted that the addition of oleic acid to metal-amide precursors results in the formation of metal oxides and dimethyl oleamides (Fig. 2b **Supplementary Fig. 48**).

We combined these two reactions to propose a scheme for the growth of metal oxides that displaces all the native ligands and generates a fully inorganic interface between the NC and the oxide shell without loss of colloidal stability (Fig. 2c). In the first half-reaction, the transamidated precursor efficiently replaces all the native oleate ligands through an amidation reaction to form oleamide and bound gallium-

amides. Then, oleic acid is added to induce the release of secondary amines by forming gallium oleate through a protic exchange with the bound amides, effectively regenerating a bound oleate surface while completing the second half reaction and representing a full c-ALD cycle. In the following c-ALD cycles, the newly passivating oleates are converted into oleamide by the transaminated precursors, and a second metal oxide bond forms, permitting the growth of a second metal oxide layer. These steps can be repeated arbitrarily as each addition involves the positioning of a long chained aliphatic tail on the surface of the NC. Further, the evolved byproducts are alkyl oleamides and secondary amines, two species that interact weakly with the NC surface,⁴¹ and therefore should not interfere with the process.

We tracked the complete process through a suite of solution NMR techniques (Fig. 3, **Supplementary Figs. 49–54**) to confirm the proposed mechanism. As a first step, the transamidated gallium precursor was added to a suspension of PbS NCs. ¹H NMR revealed the partial transformation of native oleates to alkyl oleamide through the emergence of narrow alkene resonances (**Supplementary Fig. 49**). A variable-temperature (VT) NMR experiment was performed to promote the full replacement of oleates and revealed that all the oleates are replaced after reaching 70°C (Fig. 3a). Concurrently, a very broad resonance arises (Fig. 3b), which is associated with bound Ga-didodecylamides. Diffusion ordered NMR spectroscopy (DOSY) and nuclear Overhauser effect spectroscopy (NOESY) further confirmed the anchoring of gallium amides to the NC surface and the completion of the first half reaction (**Supplementary Fig. 49**). Presence of excess precursor does not result in further reactions, suggesting the reaction is self-limiting (**Supplementary Fig. 50**). Importantly, the NCs remained colloiddally stable despite all the native oleates having been replaced by a Ga-amide terminated surface.

Upon introduction of oleic acid, the signal arising from bound gallium-didodecylamide is lost and a bound oleate resonance is reestablished in the ¹H NMR spectrum (Figs. 3a-b, **Supplementary Fig. 51**). We note that this resonance is upfield compared to the original PbS bound oleates, and is consistent with oleates being bound to a metal oxide.⁴¹ DOSY and NOESY further confirm this assignment. These steps were repeated twice and tracked, showing a similar behavior (Figs. 3a-b, **Supplementary Figs. 52–55**). This demonstration confirms that our methodology proceeds as intended, *i.e.* by alternating the surface ligands between bound oleates and bound amides (Fig. 3c). Thus, this approach should be growing metal oxides on the surface of PbS NCs.

Figure 4 displays high-angle annular dark field- scanning transmission electron microscopy (HAADF-STEM) images with the corresponding energy dispersive X-Ray spectroscopy (EDXS) elemental maps of different NCs upon the growth of gallium or titanium oxide shells. After shell growth of both metal oxides, PbS nanocubes retain their shape and size, while EDXS elemental maps confirm the spatial co-localization of both Pb and the gallium or titanium, and the presence of a shell (Fig. 4a-f; PbS spheres are presented in **Supplementary Fig. 56**). We applied the same approach to oleate passivated NaGdF₄ NCs, InP NCs and CdSe NPLs to generalize the growth procedure (Fig. 4g,h, **Supplementary Fig. 57–59**). Further, optical characterization confirmed that the InP and CdSe cores are unaffected by the growth of

metal oxides (**Supplementary Fig. 60–61**). These results evidence the generalizability of this procedure to a variety of oleate passivated nanocrystalline compositions.

Using PbS nanocubes as our benchmark, we then sought to investigate the structure of the gallium oxide shell and its evolution during the growth. High-resolution X-ray diffraction (HR-XRD) analysis revealed no significant alteration to the PbS lattice (**Supplementary Fig. 63**). Further, the absence of additional diffraction peaks suggested that the gallium oxide shell is amorphous. We then performed XAS at the Ga K, Pb L2 and Pb L3 edges of PbS nanocubes having undergone one, three and five cycles of growth. The Pb L2 and L3 X-ray absorption near edge structure (XANES) revealed no significant alteration throughout any step in the growth process (**Supplementary Fig. 64**). Together with the XRD analysis, these data suggest that the grown gallium oxide is amorphous and does not induce surface oxidation or any measurable geometric strain to the PbS lattice.

Looking at the Ga K-edge XANES, the spectral line shape evolves towards gallium oxide nucleated by directly mixing the transamidated TDMA-Ga and oleic acid as more cycles are performed (Fig. 5a, **Supplementary Fig. 48, 65**). Extended X-ray absorption fine structure (EXAFS) analysis revealed clear changes during the growth of the shell (Fig. 5b, **Supplementary Figs. 66–67, Table 1**). First, the EXAFS of PbS nanocubes that have undergone only one cycle is consistent with the presence of O (first shell, $r: 1.96\text{\AA}$), Ga (second shell, $r: 3.01\text{\AA}$) and Pb (third shell, $r: 3.91\text{\AA}$) scattering, but shows no evidence for a direct Ga-S bond. The absence of interactions with sulfur indicates that the anchoring of the first layer of gallium oxide is through the surface ligands rather than through undercoordinated sulfur sites. Furthermore, the third shell in the EXAFS is dominated by Pb-Ga scattering rather than by Ga-Ga. This Pb-Ga scattering fades as more cycles are performed and becomes better described by Ga-Ga scattering. Concomitantly, principle component analysis (PCA, **Supplementary Figs. 68–69**) indicated that the Ga K-edge XAS of PbS nanocubes after one cycle is consistent with a single component. Based on the EXAFS, we associate this component to gallium being a monolayer away to Pb. This component decreases from near unity to $\sim 30\%$ and $\leq 5\%$ for the three and five cycles, respectively, while a second spectroscopic component associated with Ga-Ga scattering emerges. The EXAFS analysis also suggests a transition in the configuration of gallium atoms being closer to octahedral in the first cycle and leaning more towards tetrahedral as the shell grows (**Supplementary Table 1**). This result additionally emphasizes that the first layer is distinct and strongly influenced by the underlying PbS. Structurally the grown metal-oxide appears to be fully amorphous, yet its local structure might find similarities with the disordered γ -Ga_{2.67}O₄ phase.^{45–48}

On the basis of all the above observations, we propose a plausible mechanism for the formation of the metal oxide shells initiated by ligand-modified precursors (Fig. 6). Starting with a carboxylate-functionalized surface (Fig. 6a), the first cycle results in the nucleation of a monolayer of gallium-oxygen species through the amidation of bound oleates by the metal amide precursor, with each metal likely anchoring with one or two surface sites (Fig. 6b). The formation of such monolayers is consistent with the self-limited nature of the proposed c-ALD process (**Supplemental Note 2**). During the following cycles, the growth likely proceeds by a continuous linear extension of gallium-oxygen species which merge to

form the extended three-dimensional highly disordered gallium oxide network that propagates away from the surface (Fig. 6c).

Overall, the self-limiting character of the process allows for the layer-by-layer growth of fully inorganic metal oxide coatings of NCs while preserving their colloidal stability. Consequently, the presented c-ALD methodology is unique compared to the alternative metal oxide coating strategies (**Supplementary Note 3**).

Conclusions

In conclusion, we have developed a new c-ALD method which creates fully inorganic metal oxide shells around NC core while preserving their colloidal stability. Crucial to this achievement is the use of reactive and colloidally stabilizing ligand-modified precursors.

The proposed mechanism only requires a carboxylate surface passivation, thus there are strong reasons to believe that the growth of metal oxide shells by c-ALD is extendable to various nanocrystalline composition such as metal chalcogenides, metal pnictogens and metal oxides as well as lanthanide doped inorganic nanoparticles and halide perovskites. Further, metal-amide precursors exist for a wide variety of metals^{20,49} and, consequently, a large library of metal oxide shelled nanocrystal compositions should be readily attainable by this method.

In addition, our treatment offers several possibilities beyond the growth of metal oxide shells. For instance, the proposed mechanism can be employed to introduce well-controlled and variable concentration of surface dopants via tuning the amount of initially anchored metal (e.g. Ga, Ti). Lastly, the formation of metal-amide terminated surface offers a new playground for surface modification as the introduction of a stoichiometric amount of carboxylic acids results in their exchange on the surface without inducing a dynamic equilibrium.

The mild conditions required, combined with the simplicity, scalability and generalizable nature of this method allow for a smooth transition of fundamental concepts and applications of gas phase ALD to their colloidal counterpart.

Declarations

Acknowledgments

This publication was created as part of NCCR Catalysis (grant number 180544), a National Centre of Competence in Research funded by the Swiss National Science Foundation. The authors thank Aurélien Bornet, Pascal Schouwink, Stefano Checchia, Alexander Chen and Andreas Dueholm Bertelsen for their insight into the NMR, TEM and XRD measurements, respectively. The staff at the BM28 (XmaS) beamline at the European Synchrotron Radiation Facility (ESRF) in Grenoble are acknowledged for their support. Access to the beamline was granted through the ESRF under proposal CH-6790.

Authors contributions

P.B.G designed and performed all experiments with assistance from others. O.S.L assisted with synthesis and NMR experiments. O.S.L, P.P.A and J.L helped in the design and interpretation of the c-ALD mechanism. M.A.N performed XAS analysis. K.K, C.B and A.L took HAADF-STEM images. P.B.J.T. acquired XAS and XRD data. O.S.L., P.P.A. and A.L. acquired XPS data. P.B.G. and R.B. wrote the manuscript. All authors revised and approved the manuscript.

Competing interests

The author declares no competing interest.

References

1. George, S. M. Atomic Layer Deposition: An Overview. *Chem. Rev.* **110**, 111–131 (2010).
2. Johnson, R. W., Hultqvist, A. & Bent, S. F. A brief review of atomic layer deposition: from fundamentals to applications. *Materials Today* **17**, 236–246 (2014).
3. Ritala, M. *et al.* Atomic Layer Deposition of Oxide Thin Films with Metal Alkoxides as Oxygen Sources. *Science* **288**, 319–321 (2000).
4. Ithurria, S. & Talapin, D. V. Colloidal Atomic Layer Deposition (c-ALD) using Self-Limiting Reactions at Nanocrystal Surface Coupled to Phase Transfer between Polar and Nonpolar Media. *J. Am. Chem. Soc.* **134**, 18585–18590 (2012).
5. Nasilowski, M., Nienhaus, L., Bertram, S. N. & Bawendi, M. G. Colloidal atomic layer deposition growth of PbS/CdS core/shell quantum dots. *Chem. Commun.* **53**, 869–872 (2017).
6. Liu, M. *et al.* Colloidal quantum dot electronics. *Nat Electron* **4**, 548–558 (2021).
7. Liu, Y. *et al.* PbSe Quantum Dot Field-Effect Transistors with Air-Stable Electron Mobilities above $7 \text{ cm}^2 \text{ V}^{-1} \text{ s}^{-1}$. *Nano Lett.* **13**, 1578–1587 (2013).
8. Pourret, A., Guyot-Sionnest, P. & Elam, J. W. Atomic Layer Deposition of ZnO in Quantum Dot Thin Films. *Advanced Materials* **21**, 232–235 (2009).
9. Trejo, O. *et al.* Quantifying Geometric Strain at the PbS QD-TiO₂ Anode Interface and Its Effect on Electronic Structures. *Nano Lett.* **15**, 7829–7836 (2015).
10. Trejo, O. *et al.* Elucidating the Evolving Atomic Structure in Atomic Layer Deposition Reactions with in Situ XANES and Machine Learning. *Chem. Mater.* **31**, 8937–8947 (2019).
11. Lojudice, A., Segura Lecina, O., Bornet, A., Luther, J. M. & Buonsanti, R. Ligand Locking on Quantum Dot Surfaces via a Mild Reactive Surface Treatment. *J. Am. Chem. Soc.* **143**, 13418–13427 (2021).
12. Orfield, N. J. *et al.* Kinetics and Thermodynamics of Killing a Quantum Dot. *ACS Appl. Mater. Interfaces* **12**, 30695–30701 (2020).

13. Ihly, R., Tolentino, J., Liu, Y., Gibbs, M. & Law, M. The Photothermal Stability of PbS Quantum Dot Solids. *ACS Nano* **5**, 8175–8186 (2011).
14. Loiudice, A., Strach, M., Saris, S., Chernyshov, D. & Buonsanti, R. Universal Oxide Shell Growth Enables in Situ Structural Studies of Perovskite Nanocrystals during the Anion Exchange Reaction. *J. Am. Chem. Soc.* **141**, 8254–8263 (2019).
15. Park, N. *et al.* Colloidal, Room-Temperature Growth of Metal Oxide Shells on InP Quantum Dots. *Inorg. Chem.* acs.inorgchem.3c00161 (2023) doi:10.1021/acs.inorgchem.3c00161.
16. Albertini, P. P. *et al.* Hybrid Oxide Coatings Generate Stable Cu Catalyst for CO₂ Electroreduction. *Just accepted Nature Materials* (2023) doi:10.21203/rs.3.rs-2873572/v1.
17. Green, P. B., Lecina, O. S., Albertini, P. P., Loiudice, A. & Buonsanti, R. Colloidal-ALD-Grown Metal Oxide Shells Enable the Synthesis of Photoactive Ligand/Nanocrystal Composite Materials. *J. Am. Chem. Soc.* jacs.3c01439 (2023) doi:10.1021/jacs.3c01439.
18. Tang, J. *et al.* Colloidal-quantum-dot photovoltaics using atomic-ligand passivation. *Nature Mater* **10**, 765–771 (2011).
19. Leskelä, M. & Ritala, M. Atomic layer deposition (ALD): from precursors to thin film structures. *Thin Solid Films* **409**, 138–146 (2002).
20. Miikkulainen, V., Leskelä, M., Ritala, M. & Puurunen, R. L. Crystallinity of inorganic films grown by atomic layer deposition: Overview and general trends. *Journal of Applied Physics* **113**, 021301 (2013).
21. McDonald, S. A. *et al.* Solution-processed PbS quantum dot infrared photodetectors and photovoltaics. *Nature Mater* **4**, 138–142 (2005).
22. Kessler, M. L. & Dempsey, J. L. Mapping the Topology of PbS Nanocrystals through Displacement Isotherms of Surface-Bound Metal Oleate Complexes. *Chem. Mater.* **32**, 2561–2571 (2020).
23. Won, Y.-H. *et al.* Highly efficient and stable InP/ZnSe/ZnS quantum dot light-emitting diodes. *Nature* **575**, 634–638 (2019).
24. Jang, E., Kim, Y., Won, Y.-H., Jang, H. & Choi, S.-M. Environmentally Friendly InP-Based Quantum Dots for Efficient Wide Color Gamut Displays. *ACS Energy Lett.* **5**, 1316–1327 (2020).
25. Zhu, Z.-J. *et al.* Stability of quantum dots in live cells. *Nature Chem* **3**, 963–968 (2011).
26. Wang, F., Deng, R. & Liu, X. Preparation of core-shell NaGdF₄ nanoparticles doped with luminescent lanthanide ions to be used as upconversion-based probes. *Nat Protoc* **9**, 1634–1644 (2014).
27. Green, P. B. *et al.* Controlling Cluster Intermediates Enables the Synthesis of Small PbS Nanocrystals with Narrow Ensemble Line Widths. *Chem. Mater.* **32**, 4083–4094 (2020).
28. Calcabrini, M. *et al.* Exploiting the Lability of Metal Halide Perovskites for Doping Semiconductor Nanocomposites. *ACS Energy Lett.* **6**, 581–587 (2021).
29. Hanrahan, M. P., Stein, J. L., Park, N., Cossairt, B. M. & Rossini, A. J. Elucidating the Location of Cd²⁺ in Post-synthetically Treated InP Quantum Dots Using Dynamic Nuclear Polarization ³¹P and ¹¹³Cd Solid-State NMR Spectroscopy. *J. Phys. Chem. C* **125**, 2956–2965 (2021).

30. Riedinger, A. *et al.* An intrinsic growth instability in isotropic materials leads to quasi-two-dimensional nanoplatelets. *Nature Mater* **16**, 743–748 (2017).
31. Hens, Z. & Martins, J. C. A Solution NMR Toolbox for Characterizing the Surface Chemistry of Colloidal Nanocrystals. *Chem. Mater.* **25**, 1211–1221 (2013).
32. Parsons, G. N. *et al.* Mechanisms and reactions during atomic layer deposition on polymers. *Coordination Chemistry Reviews* **257**, 3323–3331 (2013).
33. Biswas, M., Libera, J. A., Darling, S. B. & Elam, J. W. New Insight into the Mechanism of Sequential Infiltration Synthesis from Infrared Spectroscopy. *Chem. Mater.* **26**, 6135–6141 (2014).
34. Waldman, R. Z. *et al.* Sequential Infiltration Synthesis of Electronic Materials: Group 13 Oxides via Metal Alkyl Precursors. *Chem. Mater.* **31**, 5274–5285 (2019).
35. Berman, D. *et al.* Sequential Infiltration Synthesis for the Design of Low Refractive Index Surface Coatings with Controllable Thickness. *ACS Nano* **11**, 2521–2530 (2017).
36. Ho, T.-L. Hard soft acids bases (HSAB) principle and organic chemistry. *Chemical Reviews* **75**, 1–20 (1975).
37. Imhoff, D. W., Simeral, L. S., Sangokoya, S. A. & Peel, J. H. Characterization of Methylaluminumoxanes and Determination of Trimethylaluminum Using Proton NMR. *Organometallics* **17**, 1941–1945 (1998).
38. Chen, P. E., Anderson, N. C., Norman, Z. M. & Owen, J. S. Tight Binding of Carboxylate, Phosphonate, and Carbamate Anions to Stoichiometric CdSe Nanocrystals. *J. Am. Chem. Soc.* **139**, 3227–3236 (2017).
39. Brown, N. J. *et al.* From Organometallic Zinc and Copper Complexes to Highly Active Colloidal Catalysts for the Conversion of CO₂ to Methanol. *ACS Catal.* **5**, 2895–2902 (2015).
40. Segura Lecina, O. *et al.* Colloidal-ALD-Grown Hybrid Shells Nucleate via a Ligand–Precursor Complex. *J. Am. Chem. Soc.* **144**, 3998–4008 (2022).
41. De Roo, J., Van Driessche, I., Martins, J. C. & Hens, Z. Colloidal metal oxide nanocrystal catalysis by sustained chemically driven ligand displacement. *Nature Mater* **15**, 517–521 (2016).
42. Lundberg, H. *et al.* Mechanistic Elucidation of Zirconium-Catalyzed Direct Amidation. *J. Am. Chem. Soc.* **139**, 2286–2295 (2017).
43. Zherebetsky, D. *et al.* Hydroxylation of the surface of PbS nanocrystals passivated with oleic acid. *Science* **344**, 1380–1384 (2014).
44. Yarema, M. *et al.* Monodisperse Colloidal Gallium Nanoparticles: Synthesis, Low Temperature Crystallization, Surface Plasmon Resonance and Li-Ion Storage. *J. Am. Chem. Soc.* **136**, 12422–12430 (2014).
45. Sharma, A., Varshney, M., Shin, H.-J., Chae, K. H. & Won, S. O. Investigation on cation distribution and luminescence in spinel phase γ -Ga_{3- δ} O₄: Sm nanostructures using X-ray absorption spectroscopy. *RSC Adv.* **7**, 52543–52554 (2017).

46. Chen, Z. *et al.* Nature of GaO_x Shells Grown on Silica by Atomic Layer Deposition. *Chem. Mater.* acs.chemmater.3c00923 (2023) doi:10.1021/acs.chemmater.3c00923.
47. Roy, R., Hill, V. G. & Osborn, E. F. Polymorphism of Ga₂O₃ and the System Ga₂O₃-H₂O. *Journal of the American Chemical Society* **74**, (1952).
48. Castro-Fernández, P. *et al.* Atomic-scale changes of silica-supported catalysts with nanocrystalline or amorphous gallia phases: implications of hydrogen pretreatment on their selectivity for propane dehydrogenation. *Catal. Sci. Technol.* **12**, 3957–3968 (2022).
49. He, M., Protesescu, L., Caputo, R., Krumeich, F. & Kovalenko, M. V. A General Synthesis Strategy for Monodisperse Metallic and Metalloid Nanoparticles (In, Ga, Bi, Sb, Zn, Cu, Sn, and Their Alloys) via in Situ Formed Metal Long-Chain Amides. *Chem. Mater.* **27**, 635–647 (2015).

Figures

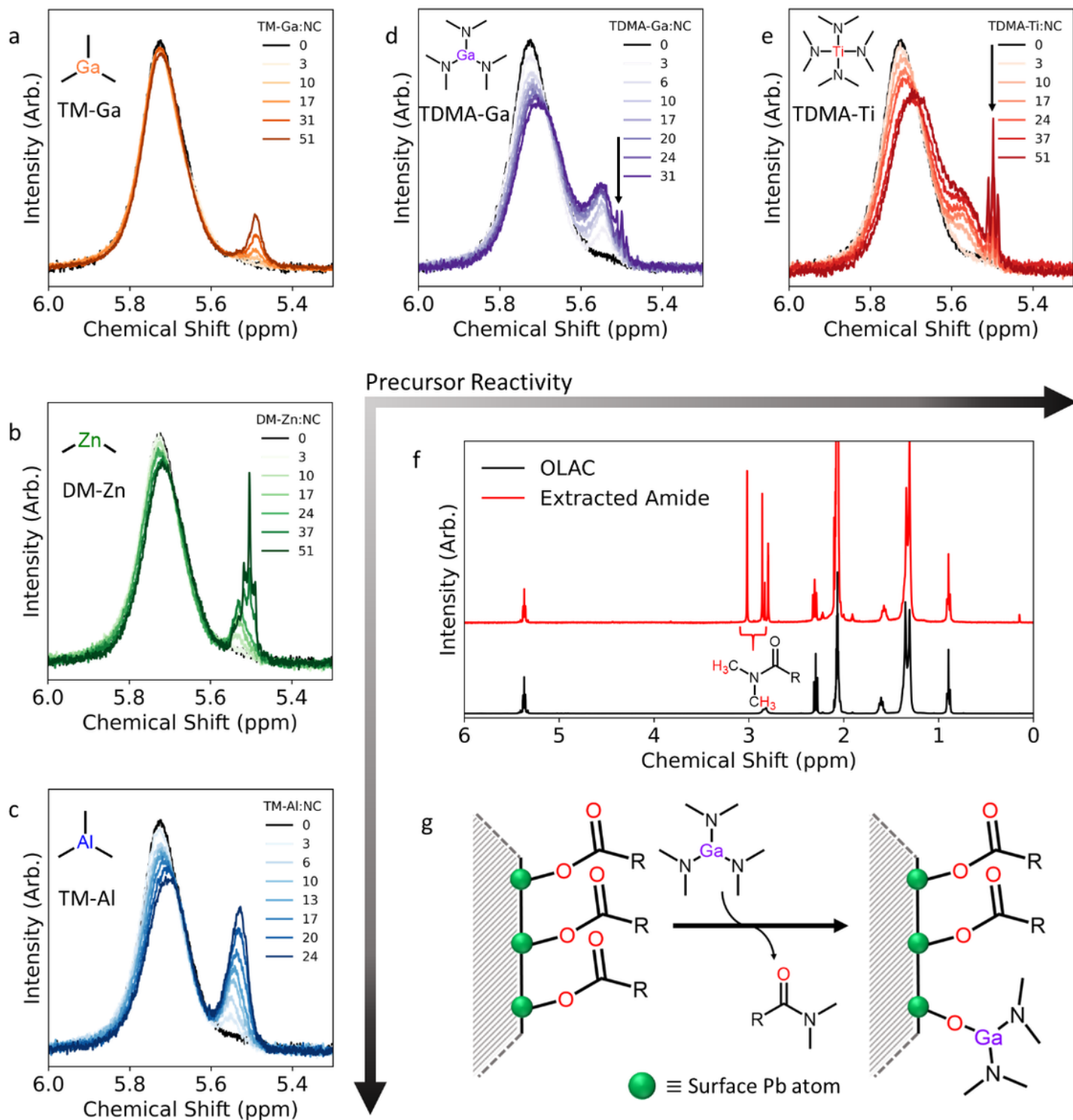


Figure 1

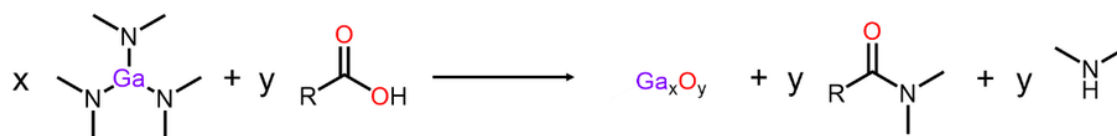
Probing the reactivity of c-ALD precursors with the oleate ligands of PbS NCs. ^1H NMR spectra tracking the alkene resonance of bound oleates through the titration of (a) TM-Ga, (b) DM-Zn, (c) TM-Al, (d) TDMA-Ga and (e) TDMA-Ti, at increasing metal precursor: NC ratio. Metal amide precursors result in the emergence of sharp resonances indicated by an arrow (d, e). (f) ^1H NMR of the isolated species compared to oleic acid (OLAC) indicates that dimethyl-oleamide is formed. (g) Representative schematic

of the surface amidation reaction occurring between metal-amide precursors and the oleate-passivated NC surface which results in the formation of a Pb-O-M bond on the NC surface and free dimethyl-oleamide. The scheme uses TDMA-Ga as a representative example. We note that direct anchoring can also occur on surface hydroxyls (**Supplementary Note 2**), which are likely present on the surface along with oleates.⁴³

a Transamidation



b Metal oxide formation



c Metal-amide based c-ALD

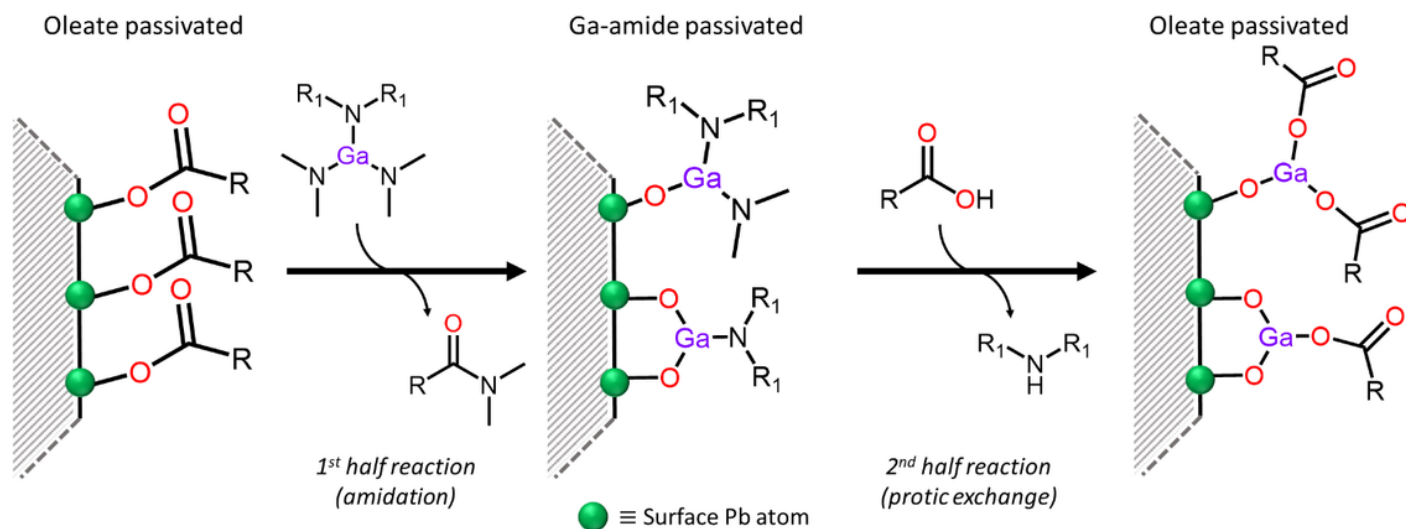


Figure 2

Schematics of the reactions employed in the c-ALD via reactive and colloiddally stabilizing precursors. (a)

A transamidation reaction is used to replace short colloiddally destabilizing dimethyl amides with longer alkyl-amides. (b) Gallium oxide synthesis from the reaction of metal-amide precursors and carboxylic acids. (c) The addition of transamidated precursors to the NC suspension results in the complete replacement of the native oleates by Ga-amides. The subsequent addition of oleic acid releases an amine and forms a Ga-oleate surface mimicking the initial oleate surface. These steps can be repeated arbitrarily to form a metal oxide shell. The scheme uses TDMA-Ga as a representative example.

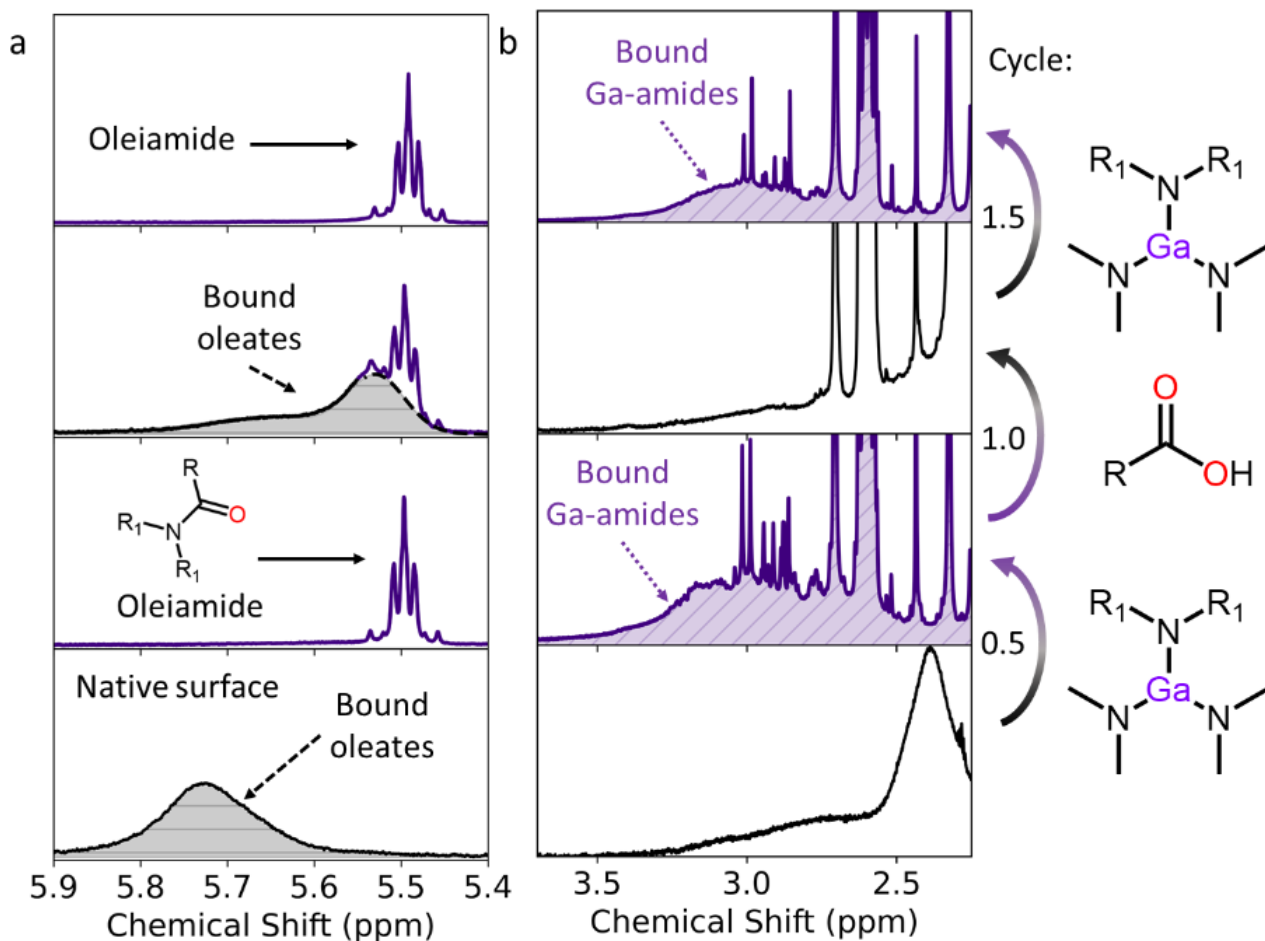


Figure 3

Monitoring the nucleation and growth of gallium oxide on the surface of PbS NCs. ^1H NMR of the oleate alkene (a) and precursor amide region (b), tracking the conversion from bound oleate (black) to bound Ga-amide and unbound oleamide (purple) during one and a half c-ALD cycles. Starting with the first half reaction (0.5 cycle), the transamidated TDMA-Ga converts bound oleates into oleamide (a). Concurrently, a bound Ga-amide (purple) resonance emerges around 3 ppm (b). Continuing with the second half

reaction (1.0 cycle) introducing oleic acid restores a bound oleate contribution (a) and results in the disappearance of bound Ga-amides (b). Starting the next cycle (1.5 cycle), the transamidated TDMA-Ga once again initiates the conversion of bound oleates to oleamide (a) and bound Ga-amide (b). These steps can be repeated as demonstrated in **Supplementary Figs. 49-55**. (c) Schematic representation of the surface chemistry throughout each half reaction alternating between a bound oleate and bound Ga-amide surface. Grey spheres indicate Pb if $n \leq 0.5$ and Ga otherwise (n represents integers starting with $n=1$).

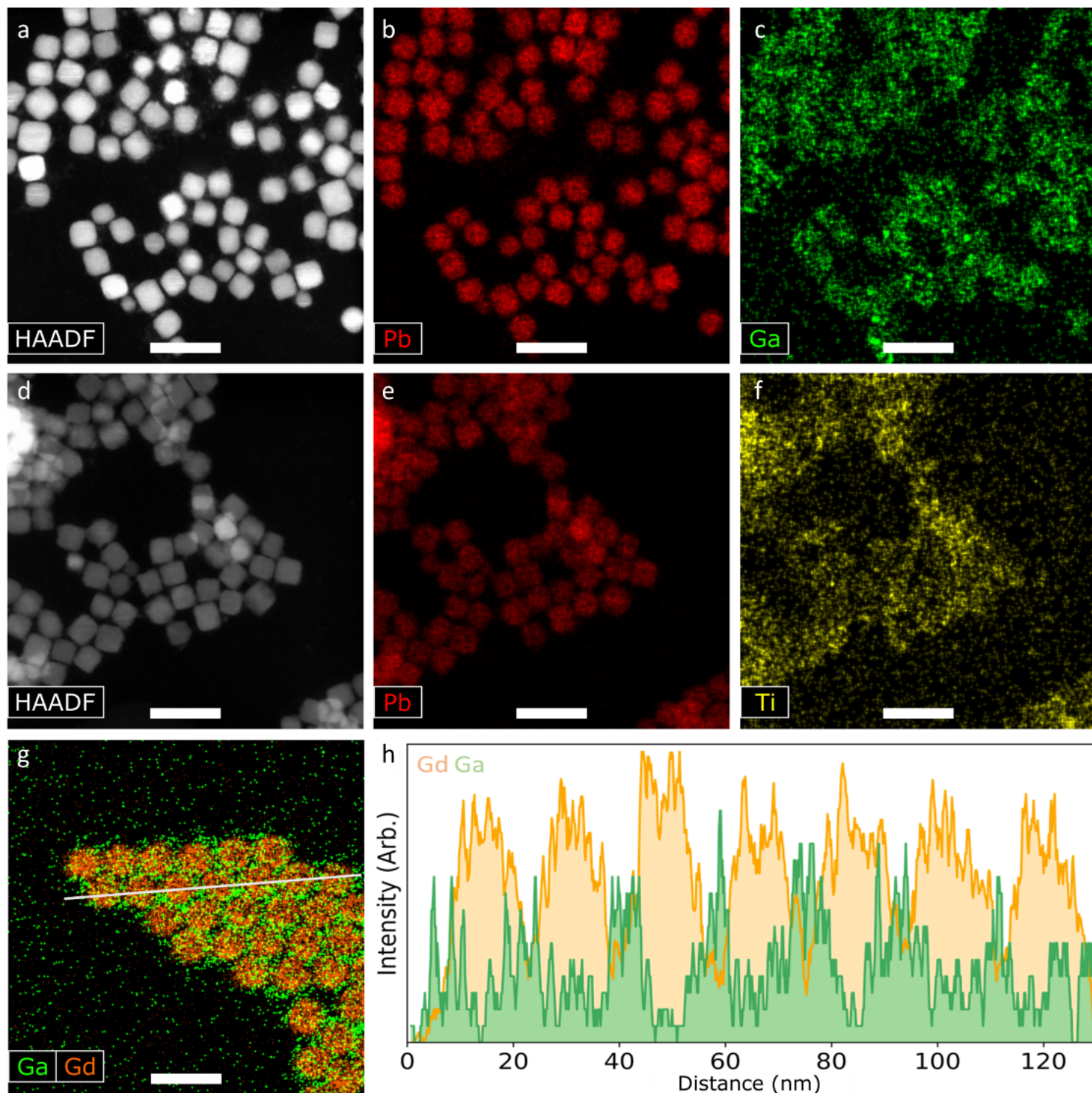


Figure 4

Observing metal-oxide shells grown on oleate capped nanocrystals. HAADF-STEM and EDXS elemental maps of PbS nanocubes with (a-c) gallium and (d-f) titanium oxide shells. (g) Superposition of the Ga and Gd contributions in an EDXS elemental map of gallium oxide shelled NaGdF₄ NCs. (h) Line scan through seven NaGdF₄ NCs shelled by gallium oxide. Scalebars are 30 nm.

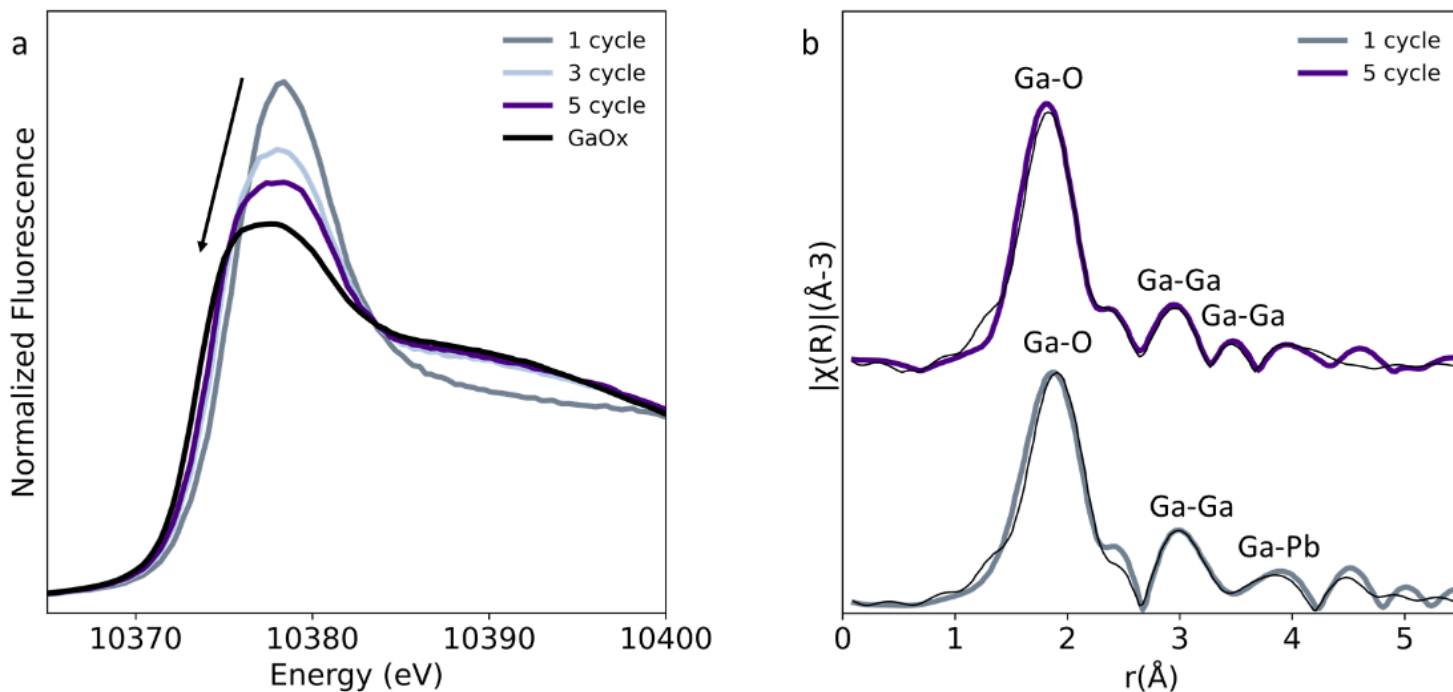


Figure 5

Structural evolution of the oxide shell during the growth. (a) Ga-K edge XANES of PbS nanocubes having undergone one, three and five cycles of c-ALD to grow a gallium oxide shell. The XANES spectra move towards that of gallium oxide (GaO_x) during the growth. This GaO_x reference was grown by reacting the transamidated TDMA-Ga with oleic acid. (b) k^2 weighted Ga K-edge EXAFS and their fitting for the same samples with one and five cycles of growth.

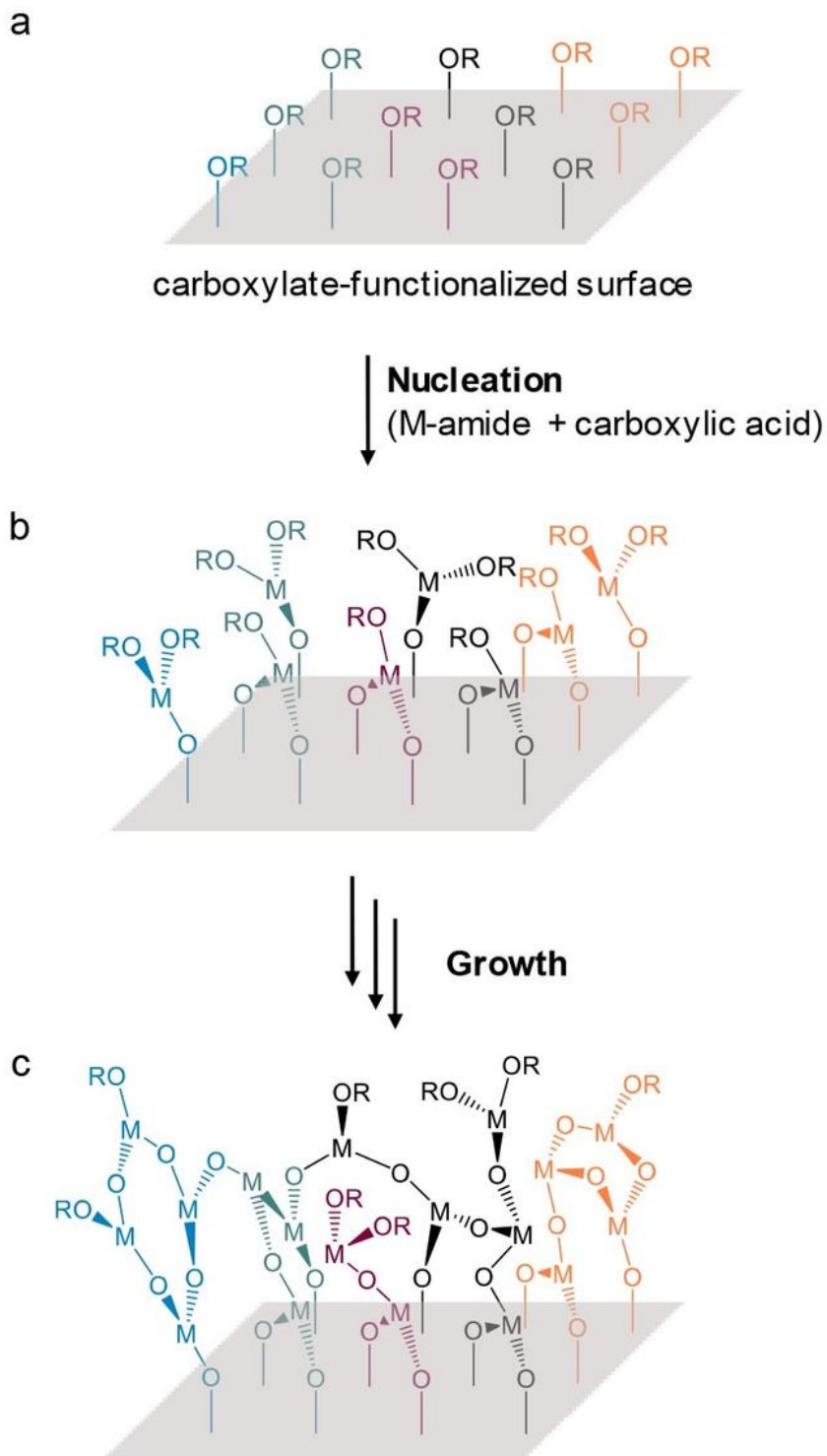


Figure 6

Proposed formation mechanism of the metal oxide coating by c-ALD via ligand modified precursors. A carboxylate functionalized surface (a) is exposed sequentially to a transamidated metal amide precursors and to carboxylic acid. Nucleation occurs through the formation of metal-oxide species arranged in one single layer (b). As more cycles are performed, a linear extension and merging of the metal oxide species form the amorphous oxide 3D structure (c). For simplicity, these schemes do not

include the complete coordination network and OR is used to represent bound oleates. Colors indicate different extensions of the metal oxide network.

Supplementary Files

This is a list of supplementary files associated with this preprint. Click to download.

- [ligandbasedcALDv8.0SI.docx](#)